

Design and Implementation of Fuzzy-Mode-Based Fault Isolation and Fault-Tolerant Control for Aircraft Electric Braking Systems

Yiyun Zhao, Zheng Wu, Fanbiao Li, *Senior Member, IEEE*, Tao Yang, *Senior Member, IEEE*, Chunhua Yang, *Fellow, IEEE*, Weihua Gui, *Member, IEEE*

Abstract—This paper addresses the fault isolation, estimation, and fault-tolerant control scheme for the aircraft electric anti-skid braking system (EABS) in the presence of actuator and sensor faults. First, the inherently nonlinear dynamics of EABSs are represented by a Takagi-Sugeno (T-S) fuzzy model, incorporating immeasurable antecedent variables to capture the time-varying characteristics. Second, based on the output equivalence principle, a fuzzy observer with unmatched antecedent variables is proposed to achieve isolation and estimation of actuator and sensor faults. The designed observer can guarantee the sensitivity to specific faults while enhancing the robustness to disturbances. The estimated fault information is then utilized to develop a fault-tolerant control strategy, ensuring effective fault compensation and tracking performance. Subsequently, the design of separate and integrated frameworks for the estimation and control units is considered, taking their interaction into account to achieve state and fault isolation, estimation, fault compensation, and tracking control. Finally, hardware-in-the-loop experimental results verify the effectiveness and real-time performance of the proposed fault isolation and fault-tolerant control method, demonstrating the practical applicability of the proposed framework.

Note to Practitioners—The aircraft anti-skid braking system (ABS) is crucial for ensuring the safety during landing, taxiing, and other ground movements. This paper focuses on developing reliable fault isolation and fault-tolerant control strategies to maintain ABS performance and efficiency in the presence of faults. The proposed approach employs a fuzzy model to analyze the effects of various faults on system outputs, enabling precise fault isolation and estimation for simultaneous multiple faults. The reconstructed fault information is then integrated to enhance the fault-tolerant control mechanism. This ensures that braking performance can be maintained, even in the presence of multiple simultaneous faults, thereby enhancing system robustness and safety. Moreover, the proposed strategy holds potential applications in other safety-critical domains, such as rail transportation

and aerospace vehicles. Future research will explore the integration of historical data to further enhance the accuracy of the fault diagnostic and accommodation units.

Index Terms—Aircraft antiskid braking system, fault isolation, fault-tolerant control, T-S fuzzy system.

I. INTRODUCTION

In modern transportation, the brake system stands as an indispensable pillar in ensuring traffic safety [1]–[3]. Particularly during aircraft landing, it is accountable for decelerating the aircraft effectively and safely [4]–[6]. With advancements in aviation technology, electric anti-skid brake systems (EABSs) have emerged as the development trend for modern aircraft due to their superior response speed and precise control capabilities [7]. Compared to hydraulic power source systems, EABSs can be configured with a broader range of feedback signals and high-speed digital processing to improve brake torque regulation and anti-skid performance. Furthermore, as the field of more-electric and all-electric aircraft evolves, EABSs can be integrated with the entire aircraft power architecture, enabling efficient energy management and contributing to improved operational efficiency and reduced environmental impact [8].

The nonlinear characteristics inherent in EABS, influenced by factors like runway surface conditions, aircraft weight, fuselage velocity, and brake disc temperature, pose significant challenges in modeling, filtering, and optimization [9]. To address these challenges, T-S fuzzy models have emerged as a powerful and flexible research framework for accurately capturing complex and time-varying dynamics. By partitioning the nonlinear system into local linear regions governed by fuzzy rules, T-S models offer a precise and adaptable representation of these dynamics. Recent advancements in fuzzy logic and T-S fuzzy modeling have broadened their applicability across various control systems, including industry, automotive and aviation domains [10]–[13]. Moreover, the integrating T-S fuzzy models with modern computational techniques has enhanced real-time implementation, improving the robustness and adaptability of control strategies in dynamic environments. Despite their considerable promise, the application of T-S fuzzy models to EABS systems remains an area for requiring further exploration and development.

The complexity of modern braking systems, coupled with harsh operational conditions such as high impact and heavy load, increases the risk of system failures, potentially causing

This work was supported in part by the National Science Fund for Excellent Young Scholars of China under Grant 62222317; in part by the Major Science and Technology Projects in Hunan Province under Grant 2021GK1030; in part by the Key Research and Development Program of Hunan Province under Grant 2023GK2023; in part by the Natural Science Foundation of Hunan Province under Grant 2025JJ10007; and in part by the Postgraduate Scientific Research Innovation Project of Hunan Province under Grant CX20240212. (Corresponding author: Zheng Wu, Fanbiao Li.)

Y. Zhao, F. Li, C. Yang and W. Gui 410083, China. (e-mails: zhaoyiyun@csu.edu.cn; fanbiaoli@csu.edu.cn; ychh@csu.edu.cn; gwh@csu.edu.cn).

Z. Wu is with the School of Automation, Central South University, Changsha, 410083, China, and also with the Power Electronics, Machines and Control Group, University of Nottingham, Nottingham NG7 2RD, U.K. (e-mail: wuzheng@csu.edu.cn).

T. Yang is with the Power Electronics, Machines and Control Group, University of Nottingham, Nottingham NG7 2RD, U.K. (e-mail: Tao.Yang@nottingham.ac.uk).

unanticipated shifts in ABS dynamics. Due to the critical safety and maintainability requirements, extensive research has focused on model-based and data-driven fault isolation and estimation methods [14]–[17]. Typically, fault isolation aims to identify the type and location of a fault, while fault estimation determines the magnitude and profile of the fault signal. Component faults, particularly those in actuators [18] and sensors [19], present significant risks to system performance and stability. During high-speed braking, both actuator and sensor faults can severely compromise key components, leading to system failure or degraded performance. Specifically, sensor faults can disrupt braking force distribution, causing uneven tire wear or slip, while actuator faults can reduce braking efficiency and impact safe deceleration. Therefore, it is crucial to develop methods that consider that simultaneously address both types of faults comprehensively. Compared to single-fault methods, approaches that address the isolation and estimation of multiple faults offer a more robust and reliable solution for EABS applications.

The next critical step after fault isolation and estimation is the implementation of fault-tolerant control (or fault-resilient control), which aims to promptly mitigate and compensate for the real-time effects of faults [20]–[24]. A widely adopted technique for ABS controller design is the backstepping method, which typically decomposes the ABS into a speed loop (alternatively referred to as the slip ratio loop) and a pressure servo loop [25]–[27]. The controller design methodology adheres to a systematic progression, starting with the inner loop and progressing to the outer loop. While this approach holds promise in addressing ABS control challenges, comprehensive research on the coordinated design of control gains and analytical validation remains limited. This deficiency is particularly acute when confronted with unstructured modeling uncertainties and nonlinear fault manifestations. Compared to qualitative analyses, there remains a significant gap in developing a robust and practical theoretical framework for the quantitative stability analysis and stabilization design of ABS systems, especially in the presence of faults.

Motivated by the critical role of EABS in aviation safety and recognizing existing technological gaps, this study aims to tackle the challenges of nonlinear system modeling, fault isolation, and fault-tolerant control for EABS. T-S fuzzy models, adept at handling uncertainties and approximating complicated nonlinear dynamics with a set of linear models, present a promising solution for improving fault diagnosis and control in EABS. Recent advancements in observer design with non-matched premise variables have significantly improved fault isolation and state estimation capabilities. These methods enhance the robustness and sensitivity of observers, thereby enabling more effective fault detection and isolation. This paper addresses these critical issues by proposing a novel approach to designing fault isolation observers and fault-tolerant controllers for nonlinear EABS. The primary contributions of this paper include:

- 1) *The time-varying nonlinear dynamics of EABS are handled through the T-S model-based representation method.* This methodology enhances the capacity of the model to characterize nonlinearities, enhanced flexibility and

precision under varying operating conditions.

- 2) *This paper also addresses the fault isolation for EABS with mismatched premise variables.* By overcoming the constraint of assuming only one fault type concurrently and precise prior variable matching between the observer and system, the proposed fault diagnosis observer is capable of simultaneously estimating both actuator and sensor faults.
- 3) *The fault estimation unit and the fault-tolerant control unit for EABS are handled within a unified framework.* To address the dynamic interaction between the observer and controller, this paper proposes both a step-by-step design and an integrated single-step design method, thereby offering enhanced design flexibility.

II. EABS MODEL DYNAMICS

A. Fuselage and Wheel Dynamics

Consider the longitudinal dynamics of the aircraft fuselage and landing gear struts under a rigid frame [9], [28], [29], as illustrated in Fig. 1. By neglecting the effects of fuselage wheel load transfer and multidimensional friction saturation along with the longitudinal dynamics, the braking dynamics of the fuselage are described as follows:

$$\begin{cases} T_r - F_x - T_n - T_m = m\dot{v}_x, \\ T_r = T_i + k_v v_x, \\ F_x = \frac{1}{2}\rho C_x S_w v_x^2, \end{cases} \quad (1)$$

where T_r is the residual thrust from the engine; F_x is the aerodynamic resistance; T_n is the friction between the nose wheel and the runway; T_m is the friction between the main wheel and the runway; m is the aircraft mass; v_x is the longitudinal taxiing speed; T_i is the initial thrust from the engine; k_v is its velocity coefficient; ρ and S_w are the air density and total wing area, respectively; C_x is the aerodynamic drag coefficient of aircraft. The vertical motion and pitch dynamics, which interact synergistically with the longitudinal dynamics, are described by the following equations:

$$\begin{cases} n_1 N_1 + n_2 N_2 + F_L = mg, \\ n_1 N_1 l_1 + n_1 T_m l_h + n_2 T_n l_h = n_2 N_2 l_2 + T_r l_T, \\ F_L = \frac{1}{2}\rho C_z S_w v_x^2, \end{cases}$$

where g represents the gravitational acceleration; N_1 and N_2 stand for the vertical loads on a single main and front wheel, respectively; F_L is the aerodynamic lift; n_1 and n_2 indicate the number of main and nose wheels, respectively; l_1 and l_2 are the horizontal distances from the main and front landing gear to the center of gravity. T_m and T_n are friction force at the main and front wheels, respectively. l_T is the vertical distance from the residual thrust to the center of gravity, l_h is the initial height of the center of gravity above the ground, and C_z is the aerodynamic lift coefficient.

The dynamics of the braked main wheel are described by:

$$J_w \dot{\omega}_r = \frac{1}{n_1} T_m R - k_b P_a - B_w \omega_r, \quad (2)$$

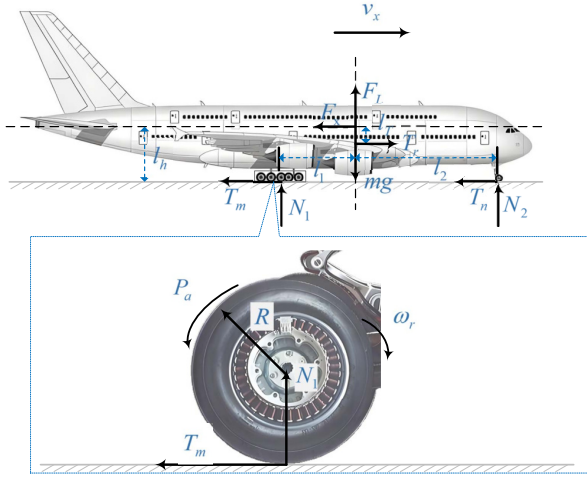


Fig. 1. Aircraft fuselage and main wheel force diagram.

where J_w is the rotational inertia of the main wheel, w_r is the angular velocity of the wheel, R is rolling radius of the wheel, k_b is the braking torque-to-pressure conversion coefficient of the braking device, P_a is the braking pressure applied to the main wheel, and B_w is damping coefficient of the wheel.

The analysis of Coulomb friction between the main and front wheels is crucial in aircraft braking:

$$T_m = \mu_m N_1, \quad T_n = \mu_n N_2, \quad (3)$$

where μ_m and μ_n are the friction coefficient at the main and nose wheels, respectively. N_1 and N_2 are normal load on the main and nose wheels, respectively.

Due to the differences in braking force and load distribution, a disparity in the frictional forces between the nose wheels μ_m and main wheels μ_n exists. The friction force on the nose wheel remains constant due to free rolling, while the main wheels experience braking pressure and are subjected to a combination of static and rolling friction. The degree of slip is indicated by the relationship between the speed of the aircraft and the linear speed of the wheels:

$$\lambda = 1 - \frac{w_r R}{v_x}.$$

where w_r is the wheel speed. The friction coefficient μ_m is related to the slip ratio λ and can be characterized by the following Magic Formula [30]:

$$\begin{aligned} \mu_m &= D_\mu \sin(C_\mu \arctan \Pi_\mu), \\ \Pi_\mu &= B_\mu \lambda - E_\mu [B_\mu \lambda - \arctan(B_\mu \lambda)], \end{aligned} \quad (4)$$

where D_μ , C_μ , B_μ and E_μ are calibration parameters related to the runway conditions.

B. Electromechanical Actuator Dynamics

The actuator of the EABSs employs an electromechanical actuator (EMA) that consists of several components, including the motor, reduction gear, ball screw, compression disc, and brake disc, as illustrated in Fig. 2. In operation, the brushless DC motor drives the reduction gear, which in turn rotates

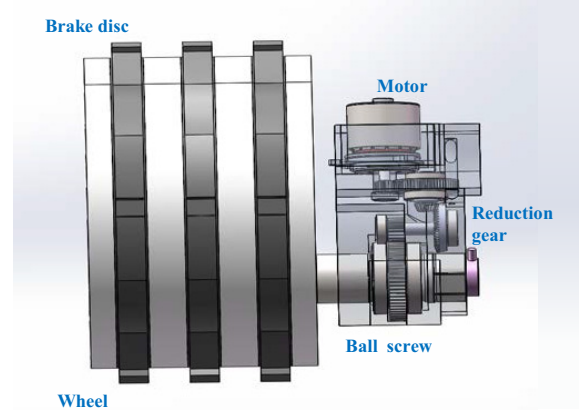


Fig. 2. Schematic diagram of EMA.

the ball screw. This rotational motion is converted into linear motion along the axis of screw, which pushes the compression disc against the brake disc. The resulting pressure generates braking torque, thereby enabling the braking mechanism. The voltage across the brushless DC motor is expressed as:

$$U_c = R_m i_e + L_e \dot{i}_e + K_e w_m, \quad (5)$$

and the electromagnetic torque is given by:

$$J_m \dot{w}_m = K_T i_e + T_L - B_v w_m, \quad (6)$$

where U_c is the voltage across the motor; R_m , i_e and L_e are the resistance, current and inductance of the motor, respectively. K_e is the electromotive force constant; w_m is the angular velocity of the motor; J_m is the rotational inertia of the motor; K_T is the torque constant of the motor; T_L is the load torque; and B_v is the viscous damping coefficient of the motor.

The braking pressure P_a can be linearly related to the displacement of the ball screw, expressed as $P_a = c_b x_e$, where c_b is the linear coefficient relating braking pressure to ball screw displacement, x_e is the displacement of the ball screw. The load force equation and the motion equation of the ball screw are given by:

$$P_a = \frac{2\pi T_L}{L_0}, \quad \dot{x}_e = \frac{L_0 w_m}{2\pi}, \quad (7)$$

where L_0 is the lead of the ball screw. By deriving P_a from equation above, the mechanical subsystem dynamics of the EMA can be expressed as:

$$\dot{P}_a = \frac{c_b L_0 w_m}{2\pi}. \quad (8)$$

Combining equations (6) and (7), the electrical subsystem equation of the EMA is obtained as:

$$\dot{w}_m = -\frac{1}{J_m} \frac{L_0}{2\pi} P_a - \frac{B_v}{J_m} w_m + \frac{K_T}{J_m} i_e. \quad (9)$$

C. T-S Fuzzy Representation

Define the state variables as $x(t) = [v_x, w_r, P_a, w_m]^T$ and the input as $u(t) = i_e$. With the above mathematical model

of the four components of the aircraft EABS and combining equations (1), (2), (8) and (9), the overall model of EABS can be expressed as:

$$\dot{x} = h_x(x, u_a, \omega), \quad y = h_y(x, f_s, \omega), \quad (10)$$

where f_a and f_s denote actuator and sensor faults, respectively, and ω represents external disturbances. $h_x(x, u_a, \omega) = [h_{v_x} \ h_{w_n} \ h_{P_a} \ h_{w_m}]^T$, $h_{v_x} = \frac{1}{m}T_r - \frac{1}{m}\mu_f N_2 - \frac{1}{m}\mu_n N_1 - \frac{1}{m}\bar{\rho}_D v_x^2 + c_1\omega$, $h_{w_n} = \frac{\mu_n N_1 r_w}{J_w} - \frac{B_w}{J_w}w_r - \frac{k_p}{J_w}P_a + c_2\omega$, $h_{P_a} = \frac{c_b L_0 w_m}{2\pi} + c_3\omega$, $h_{w_m} = -\frac{1}{J_m}\frac{L_0}{2\pi}P_a - \frac{B_w}{J_m}w_m + \frac{K_T}{J_m}u_a + c_4\omega$. N_2 and N_1 are determined by the vertical motion and pitch dynamics (2).

Remark 1: EABS actuators and sensors are susceptible to malfunctions under high temperatures and vibrations, which can lead to incorrect sensor readings and reduced braking force. Sensor failures $f_s(t)$ cause discrepancies between measured and actual values, while actuator failures $u_a(t)$ result in ineffective control. Faults can present as complete failure, jamming, constant deviation, gain issues, or combined failures, all of which significantly impact system performance and safety.

To achieve a parameterized observer design for nonlinear systems, this section proposes a fuzzy modeling approach. The longitudinal speed v_x varies within the range $v_x \in [v_{x_L}, v_{x_U}]$, where v_{x_U} denotes the upper bound (aircraft landing speed) and v_{x_L} denotes the lower bound (anti-skid brake termination speed). Consequently, $1/v_x$ falls within $[1/v_{x_U}, 1/v_{x_L}]$. According to Magic Formula (4), $\mu_m \in [\mu_{m_L}, \mu_{m_U}]$.

This paper addresses the design of fault estimation observers and controllers for nonlinear EABS adopting a fuzzy model described by IF-THEN rules. The premise variables are chosen as $\theta(t) = [\theta_1(t), \theta_2(t), \theta_3(t)]^T = [v_x, 1/v_x, \mu_m]^T$ and p -th individual plant rule is formulated as:

Model Rule p : IF θ_1 is F_{p1} , θ_2 is F_{p2} , and θ_3 is F_{p3} , THEN

$$\begin{cases} \dot{x}(t) = A_p x(t) + B(u(t) + H f_a(t)) + E\omega(t), \\ y(t) = Cx(t) + G f_s(t) + D\omega(t), \end{cases} \quad (11)$$

where F_{pi} are fuzzy sets defined as: $F_{11} = F_{21} = F_{31} = F_{41} = (v_{x_U} - v_x)/(v_{x_U} - v_{x_L})$, $F_{51} = F_{61} = F_{71} = F_{81} = (v_x - v_{x_L})/(v_{x_U} - v_{x_L})$, $F_{12} = F_{22} = F_{52} = F_{62} = (1/v_{x_L} - 1/v_x)/(1/v_{x_L} - 1/v_{x_U})$, $F_{32} = F_{42} = F_{72} = F_{82} = (1/v_x - 1/v_{x_U})/(1/v_{x_L} - 1/v_{x_U})$, $F_{13} = F_{33} = F_{53} = F_{73} = (\mu_{m_U} - \mu_m)/(\mu_{m_U} - \mu_{m_L})$, $F_{23} = F_{43} = F_{63} = F_{83} = (\mu_m - \mu_{m_L})/(\mu_{m_U} - \mu_{m_L})$. The state variables $x(t) \in \mathbb{R}^{n_x}$, control input $u(t) \in \mathbb{R}^{n_u}$, actuator fault $f_a(t) \in \mathbb{R}^{n_{f_a}}$, disturbance $\omega(t) \in \mathbb{R}^{n_\omega}$, output $y(t) \in \mathbb{R}^{n_y}$ and sensor fault $f_s(t) \in \mathbb{R}^{n_{f_s}}$ are defined accordingly. The normalized fuzzy membership function is given by:

$$\alpha_p(\theta(t)) = \eta_p(\theta(t)) / \sum_{p=1}^8 \eta_p(\theta(t)), \quad \eta_p(\theta(t)) = \prod_{i=1}^3 F_{pi}(\theta_i(t)),$$

where $\sum_{p=1}^8 \eta_p(\theta) = 1$, $n = 3$ is the number of fuzzy rules, and $m = 8$ is the number of fuzzy inference rules. Let the set be denoted as $\mathbb{J} = \{1, 2, \dots, 8\}$ to facilitate the expression.

Based on the constructed fuzzy sets and membership functions, it can be verified that the fuzzy inference model (11) is

equivalent to the original nonlinear system (10). The matrices A_p are obtained by replacing v_x , $1/v_x$, and μ_m in the matrices $A(t)$ with v_{x_L} , v_{x_U} , $\frac{1}{v_{x_L}}$, $\frac{1}{v_{x_U}}$, μ_{m_L} and μ_{m_U} according to the corresponding sets of fuzzy rules. A_p , B , H , E , C , G and D are known parameter matrices that satisfy the principle of dimensional compatibility.

The fuzzy fusion of the T-S fuzzy system (11) via defuzzification can be rewritten as

$$\begin{cases} \dot{x}(t) = \sum_{p \in \mathbb{J}} \alpha_p(\theta(t)) [A_p x(t) + B(u(t) \\ + H f_a(t)) + E\omega(t)], \\ y(t) = Cx(t) + G f_s(t) + D\omega(t). \end{cases} \quad (12)$$

The objective of this paper is to develop a fault isolation, estimation, and fault-tolerant control strategy for the nonlinear aircraft EABS by the proposed fuzzy model, addressing both actuator and sensor faults under varying operational conditions.

III. FAULT ISOLATION AND ESTIMATION OBSERVER

This section investigates the design of an asynchronous observer aimed at achieving fault isolation from sensor-affected measurement outputs, while simultaneously estimating the system states, sensor faults, and actuator faults.

A. Sensor Fault Isolation and Estimation

Sensor faults have a direct impact on system outputs, rendering the measurement and estimation of system states unreliable. To address this, simultaneous estimation of states and sensor faults is performed. Sensor faults are treated as nominal states, and an extended state vector is introduced to incorporate the effects of sensor faults into the system dynamics. The following augmented state vector is defined:

$$\bar{x}(t) = [x^T(t), f_s^T(t)]^T,$$

with the corresponding matrices defined as $\bar{A}_p \triangleq [A_p \ O]$, $\bar{T} \triangleq [I \ O]$, $\bar{C} \triangleq [C \ G]$. The input is redefined as $u_a(t) = u(t) + H f_a(t)$, which includes the nominal control input $u(t)$ and the fault-induced component $H f_a(t)$. For system described by (12), the dynamics are given by

$$\begin{cases} \bar{T} \dot{\bar{x}}(t) = \sum_{p \in \mathbb{J}} \alpha_p(\theta(t)) [\bar{A}_p \bar{x}(t) + B u_a(t) + E\omega(t)], \\ y(t) = \bar{C} \bar{x}(t) + D\omega(t). \end{cases}$$

Given that accurate measurements of the antecedent variables are unavailable, the T-S fuzzy model cannot be directly implemented for designing a fault detection observer. Instead, estimated variables, denoted as $\hat{\theta}_1(t) = \hat{v}_x$, $\hat{\theta}_2(t) = 1/\hat{v}_x$ and $\hat{\theta}_3(t) = \hat{\mu}_m$, are utilized as the premise variables of the observer fuzzy rules. This relaxation avoids the strict requirement of consistency between system and observer premise variables, making the method more robust in practical implementations. The fault detection observer is defined by the following rules:

Observer Rule q : IF $\hat{\theta}_1$ is F_{q1} , $\hat{\theta}_2(t)$ is F_{q2} , and $\hat{\theta}_3(t)$ is

F_{q3} , THEN

$$\begin{cases} \dot{z}(t) = N_q z(t) + M_q u(t) + L_q y(t), \\ \dot{\tilde{x}}(t) = z(t) + Q y(t), \\ \dot{\tilde{y}}(t) = \bar{C} \tilde{x}(t), \end{cases} \quad (13)$$

where N_q , M_q , L_q and Q are matrices to be designed. The matrices S and Q are chosen such that $S\bar{T} + Q\bar{C} = I$.

The overall observer normalization can be inferred as:

$$\begin{cases} \dot{z}(t) = \sum_{q \in \mathbb{J}} \alpha_q(\bar{\theta}(t)) [N_q z(t) + M_q u(t) + L_q y(t)], \\ \dot{\tilde{x}}(t) = z(t) + Q y(t), \\ \dot{\tilde{y}}(t) = \bar{C} \tilde{x}(t). \end{cases} \quad (14)$$

Defining the observer error $e_{\bar{x}}(t) = \bar{x}(t) - \tilde{x}(t)$ and the residual generator $e_y(t) = y(t) - \tilde{y}(t)$, we can derive the following expression:

$$\begin{aligned} \dot{e}_{\bar{x}}(t) &= \dot{\bar{x}}(t) - \dot{\tilde{x}}(t) \\ &= \sum_{p \in \mathbb{J}} \sum_{q \in \mathbb{J}} \alpha_p(\bar{\theta}(t)) \alpha_q(\bar{\theta}(t)) \{ [S\bar{A}_p - L_q \bar{C} + N_q Q \bar{C}] \bar{x}(t) \\ &\quad - N_q \tilde{x}(t) + [SB - M_q] u(t) + SBH f_a(t) \\ &\quad + [SE + N_q Q D - L_q D] \omega(t) - Q D \dot{\omega}(t) \}. \end{aligned}$$

The observer matrices are determined as follows:

$$N_q = S\bar{A}_q - W_q \bar{C}, \quad M_q = SB, \quad L_q = W_q + N_q Q, \quad (15)$$

with the actuator isolation observer error evolving as:

$$\begin{cases} \dot{e}_x(t) = \sum_{q \in \mathbb{J}} \alpha_q(\bar{\theta}(t)) \{ N_q e_{\bar{x}}(t) - Q D \dot{\omega}(t) + SBH f_a(t) \\ \quad + S \omega_{\bar{x}}(t) + [SE - W_q D] \omega(t) \}, \\ e_y(t) = \bar{C} e_{\bar{x}}(t) + D \omega(t), \end{cases} \quad (16)$$

where $\omega_{\bar{x}}(t) = \sum_{p \in \mathbb{J}} \sum_{q \in \mathbb{J}} \alpha_p(\bar{\theta}(t)) \alpha_q(\bar{\theta}(t)) [\bar{A}_p - \bar{A}_q] \bar{x}(t)$, which is norm-bounded.

The following logic criteria based on observer residuals are used to achieve sensor fault isolation:

$$\mathbb{J}_1(e_y) = \begin{cases} \geq \mathbb{J}_{1,\text{th}}, & \text{sensor fault occurrence} \\ < \mathbb{J}_{1,\text{th}}, & \text{sensor fault free} \end{cases} \quad (17)$$

where the residual monitoring function $\mathbb{J}_1(e_y) = \{ \int_{t_o}^{t_o+t_*} e_y^T(t) e_y(t) dt \}^{\frac{1}{2}}$. For the sensor fault-free case, the function can be specified by $\mathbb{J}_1(e_y) = \mathbb{J}_1(e_y)_{f_s(t)=0} \leq \varepsilon_1 \|\sigma\| \leq \mathbb{J}_{1,\text{th}}$ and $\mathbb{J}_{1,\text{th}} = \sup_{d \in \ell_2} \varepsilon_1 \|\sigma\|$, where σ represents the vector of disturbances and perturbations, and ε_1 is the scalar for observer design.

Remark 2: The augmented observer approach has gained considerable attention, with successful implementations, such as in [31]. These methods typically transform sensor faults $Gf_s(t)$ into an equivalent fault $\check{f}(t)$ for estimation. In contrast, our approach directly estimates the original sensor faults $f_s(t)$, avoiding additional transformations.

Theorem 1: Consider the fuzzy system described by (11) and the sensor fault estimation observer (14). For given scalars $\bar{\varepsilon}_1 > 0$, if there exist symmetric and positive definite matrix $P_a > 0$ and matrix \bar{W}_q , such that the following conditions

hold $\forall q \in \mathbb{J}$:

$$\bar{\Lambda} = \begin{bmatrix} \bar{\Psi}_{11} & \bar{\Psi}_{12} \\ * & \bar{\Psi}_{22} \end{bmatrix} < 0, \quad (18)$$

where

$$\begin{aligned} \bar{\Psi}_{11} &= P_a S \bar{A}_q + \bar{A}_q^T S^T P_a - \bar{W}_q \bar{C} - \bar{C}^T \bar{W}_q^T + \bar{C}^T \bar{C}, \\ \bar{\Psi}_{12} &= \Omega_p + \bar{C}^T \bar{D}, \quad \bar{\Psi}_{22} = -\bar{\varepsilon}_1 I + \bar{D}^T \bar{D}, \\ \Omega_p &= [P_a S E - \bar{W}_q D \quad -P_a Q D \quad P_a S \quad P_a S B H], \\ \bar{D} &= [D \quad O \quad O \quad O], \end{aligned}$$

then the error system (16) is asymptotically stable, and the solution of observer gain matrix W_q is given by $W_q = P_a^{-1} \bar{W}_q$.

Proof: For error dynamics system (18), consider the following Lyapunov function:

$$V_1(e_{\bar{x}}(t), t) = e_{\bar{x}}^T P_a e_{\bar{x}}(t). \quad (19)$$

Taking the time derivative of $V_1(e_{\bar{x}}(t), t)$ along the trajectories of the error dynamics (16), we obtain:

$$\begin{aligned} \dot{V}_1(e_{\bar{x}}(t), t) &= 2e_{\bar{x}}^T(t) P_a \dot{e}_{\bar{x}}(t) \\ &= \sum_{q \in \mathbb{J}} \alpha_q(\bar{\theta}(t)) 2e_{\bar{x}}^T(t) P_a \{ N_q e_{\bar{x}}(t) + SBH f_a(t) \\ &\quad - Q D \dot{\omega}(t) + S \omega_{\bar{x}}(t) + [SE - W_q D] \omega(t) \}. \end{aligned}$$

Let $\bar{\omega}(t) = [\omega^T(t), \dot{\omega}^T(t), \omega_{\bar{x}}^T(t), f_a^T(t)]^T$, and define the auxiliary function:

$$\Upsilon_1(t) = \dot{V}_1(e_{\bar{x}}(t), t) + e_y^T(t) e_y(t) - \varepsilon_1^2 \bar{\omega}^T(t) \bar{\omega}(t). \quad (20)$$

The performance index (20) can be further expressed as:

$$\begin{aligned} \Upsilon_1(t) &= \sum_{q \in \mathbb{J}} \alpha_q(\bar{\theta}(t)) \{ 2e_{\bar{x}}^T(t) N_q e_{\bar{x}}(t) + 2e_{\bar{x}}^T(t) P_a S B H f_a(t) \\ &\quad + 2e_{\bar{x}}^T(t) P_a [SE - W_q D] \omega(t) - 2e_{\bar{x}}^T(t) P_a Q D \dot{\omega}(t) \\ &\quad + 2e_{\bar{x}}^T(t) P_a S \omega_{\bar{x}}(t) \} - \varepsilon_1^2 \bar{\omega}^T(t) \bar{\omega}(t) + e_{\bar{x}}^T(t) \bar{C}^T \bar{C} e_{\bar{x}}(t) \\ &\quad + e_{\bar{x}}^T(t) \bar{C}^T D \omega(t) + \omega^T(t) D^T D \omega(t), \end{aligned}$$

Defining $\xi(t) = [e_{\bar{x}}^T(t) \quad \bar{\omega}^T(t)]^T$, the inequality can be further simplified to:

$$\Upsilon_1(t) = \sum_{q \in \mathbb{J}} \alpha_q(\bar{\theta}(t)) \{ \xi^T(t) \Lambda \xi(t) \}, \quad (21)$$

where

$$\begin{aligned} \Lambda &= \begin{bmatrix} P_a N_q + N_q^T P_a + \bar{C}^T \bar{C} & P_a \bar{E}_q + \bar{C}^T \bar{D} \\ * & -\bar{\varepsilon}_1 I + \bar{D}^T \bar{D} \end{bmatrix}, \\ \bar{E}_q &= [SE - W_q D \quad -QD \quad S \quad SBH], \quad \bar{\varepsilon}_1 = \varepsilon_1^2. \end{aligned}$$

Given the condition in (18), and using $\bar{W}_q = P_a W_q$ give rise to $\Upsilon_1(t) < 0$. The proof is completed. \blacksquare

Remark 3: The asynchronous observer design presented in this paper is capable of encompassing the results for the case where the premise variables are identically matched. In the scenario of exact matching, the observer operate synchronously with the system, which is a special case of the more general design. This point reveals that the method introduced in Theorem 1 is not only robust to mismatched premise variables, but can also be extended to the case where the premise variables are exactly matched.

B. Actuator Fault Isolation and Estimation

This section presents the design of an actuator fault isolation and estimation observer, followed by the derivation of stability conditions for the asynchronous observer.

The proposed observer structure is as follows:

$$\begin{cases} \dot{z}(t) = \sum_{q \in \mathbb{J}} \alpha_q(\bar{\theta}(t)) [N_q z(t) + M_q u(t) + \bar{H}_q \hat{f}_a(t) + L_q y(t)], \\ \ddot{x}(t) = z(t) + Qy(t), \\ \ddot{y}(t) = \bar{C}\ddot{x}(t), \\ \dot{\hat{f}}_a(t) = \sum_{q \in \mathbb{J}} \alpha_q(\bar{\theta}(t)) [V_q(y(t) - \ddot{y}(t))] + \hat{f}_a(t), \end{cases} \quad (22)$$

where matrices N_q, G_q, Q are defined as in (15), $\bar{H}_q = M_q H$, L_q and V_q are observer gains to be designed.

Defining the estimation error $e_f = f_a(t) - \hat{f}_a(t)$, we can derive the following expression:

$$\begin{cases} \dot{e}_{\bar{x}}(t) = \sum_{q \in \mathbb{J}} \alpha_q(\bar{\theta}(t)) \{N_q e_{\bar{x}}(t) - QD\dot{\omega}(t) + SBHe_f(t) \\ \quad + S\omega_{\bar{x}}(t) + [SE - W_q D]\omega(t)\}, \\ \dot{e}_f(t) = \sum_{q \in \mathbb{J}} \alpha_q(\bar{\theta}(t)) [-V_q \bar{C}e_{\bar{x}}(t) + e_f(t) + \dot{f}_a(t) \\ \quad - f_a(t) - V_q D\omega(t)], \\ e_y(t) = \bar{C}e_{\bar{x}}(t) + D\omega(t). \end{cases} \quad (23)$$

Define the augmented error state as:

$$\begin{aligned} e_{\bar{x}}(t) &= [e_{\bar{x}}^T(t), e_f^T(t)]^T, \\ \tilde{\omega}(t) &= [\omega^T(t), \dot{\omega}^T(t), \omega_{\bar{x}}^T(t), f_a^T(t), \dot{f}_a^T(t)]^T, \end{aligned}$$

then the overall dynamic system of observer error can be described as follows:

$$\begin{cases} \dot{e}_{\bar{x}}(t) = \sum_{q \in \mathbb{J}} \alpha_q(\bar{\theta}(t)) [X_q e_{\bar{x}}(t) + Z_q \tilde{\omega}(t)], \\ e_y(t) = \bar{C}e_{\bar{x}}(t) + \tilde{D}\tilde{\omega}(t), \end{cases} \quad (24)$$

where

$$\begin{aligned} X_q &= \bar{A}_q - \bar{\Gamma}_q \bar{C}, \quad Z_q = \bar{E} - \bar{\Gamma}_q \tilde{D}, \quad \tilde{C} = [\bar{C} \quad O], \\ \bar{A}_q &= \begin{bmatrix} S\bar{A}_q & SBH \\ O & I \end{bmatrix}, \quad \bar{\Gamma}_q = \begin{bmatrix} W_q \\ V_q \end{bmatrix}, \\ \bar{E} &= \begin{bmatrix} SE & -QD & S & O & O \\ O & O & O & -I & I \end{bmatrix}, \quad \tilde{D} = [\tilde{D} \quad O]. \end{aligned}$$

Similar to the previous section, the performance function $\mathbb{J}_2(e_y)$, the detection limit $\mathbb{J}_{2,th}$ and corresponding detection logic for actuator fault isolation can be set up analogously to (17).

Theorem 2: Consider the fuzzy system described by (11) and the sensor fault estimation observer (13). For given scalars $\bar{\varepsilon}_2 > 0$, if there exist symmetrical and positive definite matrix $P_b > 0$, and matrices \bar{W}_q and \bar{V}_q , such that the following conditions hold $\forall q \in \mathbb{J}$:

$$\tilde{\Lambda}_p = \begin{bmatrix} \tilde{\Psi}_{11} & \tilde{\Psi}_{12} \\ * & \tilde{\Psi}_{22} \end{bmatrix} < 0, \quad (25)$$

where

$$\begin{aligned} \tilde{\Psi}_{11} &= P_b \bar{A}_q + \bar{A}_q^T P_b - \bar{\Gamma}_q \tilde{C} - \tilde{C}^T \bar{\Gamma}_q^T + \tilde{C}^T \tilde{C}, \\ \tilde{\Psi}_{12} &= P_b \bar{E} + \tilde{C}^T \tilde{D}, \quad \tilde{\Psi}_{22} = -\bar{\varepsilon}_2 I + \tilde{D}^T \tilde{D}, \quad \bar{\Gamma}_q = [\bar{W}_q^T, \bar{V}_q^T]^T, \end{aligned}$$

then the error system (24) is asymptotically stable, and the solution of observer gain matrices W_q and V_q are given by

$$\begin{bmatrix} W_q \\ V_q \end{bmatrix} = P_b^{-1} \begin{bmatrix} \bar{W}_q \\ \bar{V}_q \end{bmatrix}.$$

Proof: Define the Lyapunov function as

$$V_2(e_{\bar{x}}(t), t) = e_{\bar{x}}^T(t) P_b e_{\bar{x}}(t), \quad (26)$$

and the auxiliary function as

$$\Upsilon_2(t) = \dot{V}_2(e_{\bar{x}}(t), t) + e_y^T(t) e_y(t) - \bar{\varepsilon}_2 \tilde{\omega}^T(t) \tilde{\omega}(t).$$

Taking the time derivative of $V_2(e_{\bar{x}}(t), t)$, we have

$$\begin{aligned} \dot{V}_2(e_{\bar{x}}(t), t) &= 2e_{\bar{x}}^T(t) P_b \dot{e}_{\bar{x}}(t) \\ &= \sum_{q \in \mathbb{J}} \alpha_q(\bar{\theta}(t)) \{2e_{\bar{x}}^T(t) P_b [\bar{A}_q - \bar{\Gamma}_q \tilde{C}] e_{\bar{x}}(t) \\ &\quad + 2e_{\bar{x}}^T(t) P_b [\bar{E} - \bar{\Gamma}_q \tilde{D}] \tilde{\omega}(t)\}. \end{aligned}$$

The remainder of the proof is derived by applying the matrix form $\bar{\Gamma}_q = P_b \bar{\Gamma}_q$ and referencing the relevant part of Theorem 1, thus completing the proof. ■

IV. FAULT-TOLERANT TRACKING CONTROLLER

The objective of this section is to fully utilize the fault information estimated in the previous section to design a controller, thereby achieving fault compensation and fault-tolerant tracking. This controller enables the EABS to operate according to a predefined deceleration rate or slip ratio.

A. Controller Design

Let the desired state trajectory be denoted as $x_r(t)$ and the corresponding output as $y_r(t) = Cx_r(t)$. The tracking error is defined as $e_r(t) = x(t) - x_r(t)$ and $e_\eta(t) = y(t) - y_r(t) - G\dot{f}_s(t)$. The time derivatives of above errors are expressed as:

$$\begin{aligned} \dot{e}_r(t) &= \sum_{p \in \mathbb{J}} \alpha_p(\theta(t)) [A_p x(t) + B(u(t) + Hf_a(t)) \\ &\quad + E\omega(t)] - \dot{x}_r(t). \end{aligned}$$

The control input is formulated as:

$$Bu(t) = Bv(t) - BH\hat{f}_a(t) - A_q x_r(t) + \dot{x}_r(t), \quad (27)$$

where $v(t)$ is the nominal control input, which is constructed based on the feedback of observer-estimated information as follows:

Controller Rule q : IF $\bar{\theta}_1$ is F_{q1} , $\bar{\theta}_2(t)$ is F_{q2} , and $\bar{\theta}_3(t)$ is F_{q3} , THEN

$$v(t) = K_q[\hat{x}(t) - x_r(t)], \quad (28)$$

where $\hat{x}(t) = \bar{T}\ddot{x}(t)$ and K_q is the gain matrix to be design.

Remark 4: The controller structure consists of three essential components, each crucial for ensuring the stability and desired performance of the closed-loop system: 1) $Bv(t)$ is applied

to stabilize the closed-loop system, 2) $H\hat{f}_a(t)$ mitigates the impact of actuator faults, and 3) $-A_q x_r(t) + \dot{x}_r(t)$ ensures accurate tracking as the system converges to the reference trajectory.

Remark 5: Considering the form of the matrix B , the practical form of the controller for $q \in \mathbb{J}$ is given by:

$$u(t) = K_q \hat{x}(t) - K_q x_r(t) - H\hat{f}_a(t) - b_4^{-1} [\underline{A}_q x_r(t) - \dot{x}_{nr}(t)].$$

where $x_r(t) = [x_{1r}^T(t), \dots, x_{nr}^T(t)]$ and $A_q = [\bar{A}_q^T \underline{A}_q^T]^T$.

By connecting the system dynamics described in (11) with the input (27) and (28), the closed-loop system can be expressed as follows:

$$\dot{e}_r(t) = \sum_{q \in \mathbb{J}} \alpha_q(\bar{\theta}(t)) \{ (A_q + BK_q) e_r(t) + I \omega_x(t) - BK_q \bar{T} e_{\bar{x}}(t) + BH e_f(t) + E \omega(t) \},$$

where $\omega_x(t) = \sum_{p \in \mathbb{J}} \sum_{q \in \mathbb{J}} \alpha_p(\theta(t)) \alpha_q(\bar{\theta}(t)) [A_p - A_q] x(t)$ is norm-bounded.

To analyze the dynamics of the estimation and tracking error, define the augmented vector as:

$$\hat{e}(t) = [e_r^T(t), e_{\bar{x}}^T(t), e_f^T(t)]^T, \quad q(t) = [e_{\eta}^T(t), e_y^T(t)]^T, \\ \hat{\omega}(t) = [\omega^T(t), \omega_x^T(t), \dot{\omega}^T(t), \omega_{\bar{x}}^T(t), f_a^T(t), \dot{f}_a^T(t)]^T, \quad (29)$$

the dynamics of the estimation and tracking errors can then be described by:

$$\begin{cases} \dot{\hat{e}}(t) = \sum_{q \in \mathbb{J}} \alpha_q(\bar{\theta}(t)) [\hat{X}_q \hat{e}(t) + \hat{Z}_q \hat{\omega}(t)], \\ q(t) = \hat{C} \hat{e}(t) + \hat{D} \hat{\omega}(t), \end{cases}$$

where the matrices are defined as:

$$\hat{X}_q = \begin{bmatrix} A_q + BK_q & -BK_q \bar{T} & BH \\ O & S\bar{A}_q - \bar{W}_q \bar{C} & SBH \\ O & -\bar{V}_q \bar{C} & I \end{bmatrix}, \\ \hat{Z}_q = \begin{bmatrix} E & I & O & O & O & O \\ SE - \bar{W}_q D & O & -QD & S & O & O \\ -\bar{V}_q D & O & O & O & -I & I \end{bmatrix}, \\ \hat{C} = \begin{bmatrix} C & \hat{G} \\ O & \hat{C} \end{bmatrix}, \quad \hat{D} = \begin{bmatrix} D & O \\ D & O \end{bmatrix}, \\ \hat{G} = [G\hat{T} \quad O], \quad \hat{T} = [O \quad I].$$

Building upon the fault estimation observer developed in the previous section, two design approaches are proposed for the dynamic output feedback observer in (22) and the controller in (28): a two-step separate design and a single-step integrated design.

B. Two-Step Separate Design

This section explores the design of fault observers and fault-tolerant controllers by a two-step procedure. The relevant

matrices can be decomposed as follows:

$$\hat{X}_q = \hat{A}_q - \hat{\Gamma}_q \check{C}, \quad \hat{Z}_q = \hat{E} - \hat{\Gamma}_q \check{D}, \\ \hat{A}_q = \begin{bmatrix} A_q + BK_q & -BK_q \bar{T} & BH \\ O & S\bar{A}_q \bar{C} & SBH \\ O & O & I \end{bmatrix}, \quad \hat{\Gamma}_q = \begin{bmatrix} O \\ W_q \\ V_q \end{bmatrix}, \\ \hat{E} = \begin{bmatrix} E & I & O & O & O & O \\ SE & O & -QD & S & O & O \\ O & O & O & O & -I & I \end{bmatrix}, \\ \check{C} = [O \quad \bar{C} \quad O], \quad \check{D} = [\bar{D} \quad O \quad O].$$

Theorem 3: Consider the system described by (11), with the extended state observer designed as in (22) and its error system given in (24), the controller synthesized as in (27) and (28). Given the parameter $\bar{\varepsilon}_3 > 0$ and an appropriate selection of the matrix K_q for $q \in \mathbb{J}$, if there exists a symmetric and positive definite matrix $P_c = \text{diag}\{P_{c1}, P_{c2}\}$, along with matrices \bar{W}_q and \bar{V}_q , such that

$$\hat{\Lambda}_p = \begin{bmatrix} \hat{\Psi}_{11} & \hat{\Psi}_{12} \\ * & \hat{\Psi}_{22} \end{bmatrix} < 0, \quad (30)$$

where

$$\hat{\Psi}_{11} = P_c \hat{A}_q + \hat{A}_q^T P_c - \check{\Gamma}_q \check{C} - \check{C}^T \check{\Gamma}_q^T + \hat{C}^T \hat{C}, \\ \hat{\Psi}_{12} = P_c \hat{E} + \hat{C}^T \hat{D}, \quad \hat{\Psi}_{22} = -\bar{\varepsilon}_3 I + \hat{D}^T \hat{D}, \quad \check{\Gamma}_q = [O, \bar{\Gamma}_q^T]^T,$$

then the error system (29) is asymptotically stable, and the solution of observer gain matrices W_q and V_q are determined by:

$$\begin{bmatrix} W_q \\ V_q \end{bmatrix} = P_{c2}^{-1} \begin{bmatrix} \bar{W}_q \\ \bar{V}_q \end{bmatrix}.$$

Proof: Consider the Lyapunov function as $V_3(\hat{e}(t), t) = \hat{e}^T(t) P_c \hat{e}(t)$ and define the auxiliary function as $\Upsilon_3(t) = \dot{V}_3(\hat{e}(t), t) + q^T(t) q(t) - \bar{\varepsilon}_3 \hat{\omega}^T(t) \hat{\omega}(t)$, where $P_c = \text{diag}\{P_{c1}, P_{c2}\}$. The derivative of $V_3(\hat{e}(t), t)$ along the trajectory of $\hat{e}(t)$ in (29), follows the similar structure as the Lyapunov function derivative in 2. The asymptotic stability of the error system is ensured by selecting appropriate observer gain matrices $\bar{\Gamma}_q = P_{c2} \bar{\Gamma}_q$, which are derived by applying the conditions of Theorem 1. ■

Remark 6: This algorithm provides a systematic approach to resolving the inequalities presented in Theorems 1 and 2.

Step 1: Set the controller gain K_q such that the matrices $A_q + BK_q$ are Hurwitz $\forall q \in \mathbb{J}$.

Step 2: Solve the inequalities (30) by the values of K_q obtained in Step 1. Following this, compute the estimation gain matrices W_q and V_q as:

$$\begin{bmatrix} W_q \\ V_q \end{bmatrix} = P_{c2} \begin{bmatrix} \bar{W}_q \\ \bar{V}_q \end{bmatrix}.$$

C. Single-Step Integrated Design

Next, the integrated design of the fault observer and fault-tolerant controller is addressed.

Theorem 4: Consider the system described by (11), with the extended state observer designed as in (22), its error system as in (24), and the controller synthesized as in (27) and (28).

Given the parameter $\gamma > 0$, $\vartheta_1 > 0$, $\vartheta_2 > 0$ and $\bar{\varepsilon}_4 = \bar{\varepsilon}_{41} + \bar{\varepsilon}_{42} > 0$, if there exists symmetric and positive definite matrix $\bar{P}_d = \text{diag}\{\bar{P}_{d1}, \bar{P}_{d2}\}$ and P_{d3} , along with matrices \check{W}_q, \check{V}_q and \check{K}_q , such that the following conditions hold:

$$\check{\Lambda}_{1p} = \begin{bmatrix} \check{\Psi}_{11}^1 & \check{\Psi}_{12}^1 \\ * & \check{\Psi}_{22}^1 \end{bmatrix} < 0, \quad (31)$$

$$\check{\Lambda}_{2p} = \begin{bmatrix} \check{\Psi}_{11}^2 & \check{\Psi}_{12}^2 \\ * & \check{\Psi}_{22}^2 \end{bmatrix} < 0, \quad (32)$$

where

$$\check{\Psi}_{11}^1 = \begin{bmatrix} \check{\Phi}_{11}^1 & \check{\Phi}_{12}^1 \\ * & \check{\Phi}_{22}^1 \end{bmatrix}, \quad \check{\Psi}_{12}^1 = \begin{bmatrix} \check{\Phi}_{13}^1 & \check{\Phi}_{14}^1 & \check{\Phi}_{15}^1 \\ O & O & O \end{bmatrix},$$

$$\check{\Psi}_{12}^2 = \begin{bmatrix} \check{\Phi}_{12}^2 & \check{\Phi}_{13}^2 \\ O & O \end{bmatrix}, \quad \check{\Psi}_{22}^2 = \begin{bmatrix} \check{\Phi}_{22}^2 & O \\ O & \check{\Phi}_{33}^2 \end{bmatrix},$$

$$\check{\Psi}_{22}^1 = \text{diag}\{\check{\Phi}_{33}^1, \check{\Phi}_{44}^1, \check{\Phi}_{55}^1\},$$

$$\check{\Phi}_{11}^1 = A_q \bar{P}_{d1} + \bar{P}_{d1} A_q^T + B \check{K}_q + \check{K}_q^T B^T,$$

$$\check{\Phi}_{12}^1 = -B \check{K}_q, \quad \check{\Phi}_{22}^1 = -\vartheta_1 \bar{P}_{d1}, \quad \check{\Phi}_{33}^1 = -\vartheta_2 P_{d3},$$

$$\check{\Phi}_{13}^1 = B H, \quad \check{\Phi}_{14}^1 = \check{E} + \bar{P}_{d1} C^T \check{D}_1, \quad \check{E} = [E \quad I],$$

$$\check{\Phi}_{44}^1 = -\bar{\varepsilon}_{41} I, \quad I_\varepsilon = \text{diag}\{\bar{\varepsilon}_{42} I, \bar{\varepsilon}_4 I\},$$

$$\check{\Phi}_{15}^1 = \bar{P}_{d1} C^T, \quad \check{\Phi}_{55}^1 = -(\gamma + 1) I,$$

$$\check{\Psi}_{11}^2 = P_{d2} \check{A}_q + \check{A}_q^T P_{d2} - \check{\Gamma}_q \check{C} - \check{C}^T \check{\Gamma}_q^T + \gamma^{-1} \hat{G}^T \hat{G} + \bar{P}_d,$$

$$\check{\Phi}_{12}^2 = P_{d2} \check{E} - \check{\Gamma}_q \check{D} + \hat{G}^T \check{D}_2 + \check{C}^T \check{D}_2, \quad \check{\Gamma}_q = [\check{W}_q^T, \check{V}_q^T]^T,$$

$$\check{\Phi}_{13}^2 = \{\vartheta_1 I, O\}, \quad \bar{P}_d = \text{diag}\{O, \vartheta_2 P_{d3}\} + \check{C}^T \check{C},$$

$$\check{\Phi}_{22}^2 = -I_\varepsilon + \check{D}_2^T \check{D}_2, \quad \check{\Phi}_{33}^2 = \vartheta_1 \bar{P}_{d1},$$

then the error system (29) is asymptotically stable, and the solutions of controller gain matrix K_q and observer gain matrices W_q and V_q are given by

$$K_q = \check{K}_q \bar{P}_{d1}^{-1}, \quad \begin{bmatrix} W_q \\ V_q \end{bmatrix} = P_{d2}^{-1} \begin{bmatrix} \check{W}_q \\ \check{V}_q \end{bmatrix}.$$

Proof: Consider the Lyapunov function:

$$V_4(\hat{e}(t), t) = \hat{e}^T(t) P_d \hat{e}(t), \quad (33)$$

and define an auxiliary function as $\Upsilon_4(t) = \dot{V}_4(\hat{e}(t), t) + q^T(t)q(t) - \varepsilon_4^2 \hat{\omega}^T(t) \hat{\omega}(t)$, where $P_d = \text{diag}\{P_{d1}, P_{d2}\}$.

Taking the derivative of $V_4(\hat{e}(t), t)$ along the solution of $\hat{e}(t)$ in (29), we obtain:

$$\begin{aligned} \dot{V}_4(\hat{e}(t), t) &= 2\hat{e}^T(t) P_d \dot{\hat{e}}(t) \\ &= \sum_{q \in \mathbb{J}} 2\alpha_q(\bar{\theta}(t)) \hat{e}^T(t) P_d [\hat{X}_q \hat{e}(t) + \hat{Z}_q \hat{\omega}(t)]. \end{aligned}$$

Substituting this into the auxiliary function $\Upsilon_4(t)$, we have

$$\begin{aligned} \Upsilon_4(t) &= \sum_{q \in \mathbb{J}} 2\alpha_q(\bar{\theta}(t)) \left\{ \hat{e}^T(t) P_d [\hat{X}_q \hat{e}(t) + \hat{Z}_q \hat{\omega}(t)] \right\} \\ &\quad + q^T(t)q(t) - \varepsilon_4^2 \hat{\omega}^T(t) \hat{\omega}(t). \end{aligned}$$

We first ensure that the following conditions hold:

$$\dot{V}_4(\hat{e}(t), t) + q^T(t)q(t) - \varepsilon_4^2 \hat{\omega}^T(t) \hat{\omega}(t) < 0, \quad (34)$$

which implies the inequality:

$$\begin{aligned} \sum_{q \in \mathbb{J}} 2\alpha_q(\bar{\theta}(t)) \left\{ \hat{e}^T(t) P_d [\hat{X}_q \hat{e}(t) + \hat{Z}_q \hat{\omega}(t)] \right\} \\ + q^T(t)q(t) - \varepsilon_4 \hat{\omega}^T(t) \hat{\omega}(t) < 0, \quad (35) \end{aligned}$$

where $\bar{\varepsilon}_4 = \varepsilon_4^2$. Define the auxiliary term:

$$\begin{aligned} \bar{\Upsilon}(t) &= \begin{bmatrix} e_{\bar{x}}^T(t) & e_f^T(t) \end{bmatrix} \begin{bmatrix} \bar{Y}_1 & O \\ O & \bar{Y}_2 \end{bmatrix} \begin{bmatrix} e_{\bar{x}}(t) \\ e_f(t) \end{bmatrix}, \\ \bar{Y}_1 &= \text{diag}\{\vartheta_1 P_{d1}, O\}, \quad \bar{Y}_2 = \vartheta_2 P_{d3}, \end{aligned}$$

where ϑ_1 and ϑ_2 are positive scalars.

Applying the matrix scaling technique, we express the quadratic term in the following form:

$$\begin{aligned} q^T(t)q(t) &\leq e_r^T(t) C^T C e_r(t) + \gamma e_r^T(t) C^T C e_r(t) \\ &\quad + \gamma^{-1} e_{\bar{x}}^T(t) \hat{G}^T \hat{G} e_{\bar{x}}(t) + e_{\bar{x}}^T(t) \check{C}^T \check{C} e_{\bar{x}}(t) \\ &\quad + 2e_r^T(t) C^T \check{D}_1 \check{\omega}(t) + 2e_{\bar{x}}^T(t) \hat{G}^T \check{D}_2 \hat{\omega}(t) \\ &\quad + 2e_{\bar{x}}^T(t) \check{C}^T \check{D}_2 \hat{\omega}(t) + \check{\omega}^T(t) \check{D}_1^T \check{D}_1 \check{\omega}(t) \\ &\quad + \hat{\omega}^T(t) \check{D}_2^T \check{D}_2 \hat{\omega}(t), \end{aligned}$$

where

$$\check{\omega}(t) = [\omega^T(t), \omega_x^T(t)]^T, \quad \check{D}_1 = [D \quad O], \quad \check{D}_2 = [D \quad O].$$

Thus, the condition is satisfied if the following inequalities hold:

$$\begin{aligned} \check{\Lambda}_1 + \check{\Lambda}_2 + e_{\bar{x}}^T(t) \bar{Y}_1 e_{\bar{x}}(t) + e_f^T(t) \bar{Y}_2 e_f(t) \\ - \vartheta_1 e_x^T(t) P_{d1} e_x(t) - \vartheta_2 e_f^T(t) P_{d3} e_f(t) < 0, \quad (36) \end{aligned}$$

where

$$\begin{aligned} \check{\Lambda}_1 &= \sum_{q \in \mathbb{J}} 2\alpha_q(\bar{\theta}(t)) \left\{ e_r^T(t) P_{d1} [(A_q + B K_q) e_r(t) - B K_q e_x(t) \right. \\ &\quad \left. + B H e_f(t) + E \omega(t) + I \omega_x(t)] \right\} + e_r^T(t) C^T C e_r(t) \\ &\quad + 2e_r^T(t) C^T \check{D}_1 \check{\omega}(t) + \gamma e_r^T(t) C^T C e_r(t) \\ &\quad + \check{\omega}^T(t) \check{D}_1^T \check{D}_1 \check{\omega}(t) - \bar{\varepsilon}_{41} \check{\omega}^T(t) \check{\omega}(t), \\ \check{\Lambda}_2 &= \sum_{q \in \mathbb{J}} 2\alpha_q(\bar{\theta}(t)) \left\{ e_{\bar{x}}^T(t) P_{d2} [(\check{A}_q - \check{\Gamma}_q \check{C}) e_{\bar{x}}(t) + (\check{E} - \check{\Gamma}_q \check{D}) \right. \\ &\quad \left. \times \hat{\omega}(t)] \right\} + \gamma^{-1} e_{\bar{x}}^T(t) \hat{G}^T \hat{G} e_{\bar{x}}(t) + e_{\bar{x}}^T(t) \check{C}^T \check{C} e_{\bar{x}}(t) \\ &\quad + 2e_{\bar{x}}^T(t) \hat{G}^T \check{D}_2 \hat{\omega}(t) + 2e_{\bar{x}}^T(t) \check{C}^T \check{D}_2 \hat{\omega}(t) \\ &\quad + \hat{\omega}^T(t) \check{D}_2^T \check{D}_2 \hat{\omega}(t) - \hat{\omega}^T(t) I_\varepsilon \hat{\omega}(t). \quad (37) \end{aligned}$$

The inequality (36) can be established when the following conditions are simultaneously satisfied:

$$\check{\Lambda}_1 - \vartheta_1 e_x^T(t) P_{d1} e_x(t) - \vartheta_2 e_f^T(t) P_{d3} e_f(t) < 0, \quad (38)$$

$$\check{\Lambda}_2 + e_{\bar{x}}^T(t) \bar{Y}_1 e_{\bar{x}}(t) + e_f^T(t) \bar{Y}_2 e_f(t) < 0. \quad (39)$$

Let $\check{\xi}_1(t) = [e_r^T(t), e_{\bar{x}}^T(t), e_f^T(t), \check{\omega}^T(t)]^T$ and $\check{\xi}_2(t) = [e_{\bar{x}}^T(t), \hat{\omega}^T(t)]^T$. The conditions can be further expressed as:

$$\sum_{q \in \mathbb{J}} \alpha_q(\bar{\theta}(t)) \check{\xi}_1^T(t) \Theta_1 \check{\xi}_1(t) < 0, \quad (40)$$

$$\sum_{q \in \mathbb{J}} \alpha_q(\bar{\theta}(t)) \check{\xi}_2^T(t) \Theta_2 \check{\xi}_2(t) < 0, \quad (41)$$

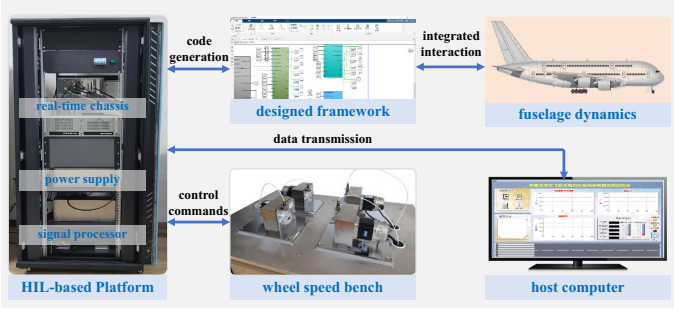


Fig. 3. Experimental block diagram.

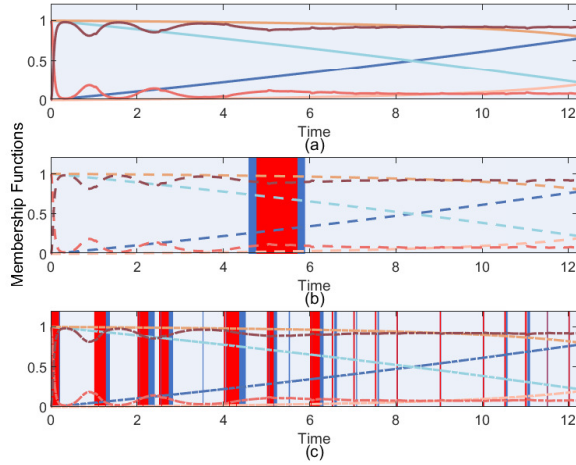


Fig. 4. Fuzzy membership functions (a), (b), and (c) are corresponding to plant, observer, and controller, respectively.

where

$$\Theta_1 = \begin{bmatrix} \Theta_{11}^1 & -P_{d1}BK_q & P_{d1}BH & \Theta_{14}^1 \\ * & -\vartheta_1 P_{d1} & O & O \\ * & * & -\vartheta_2 P_{d3} & O \\ * & * & * & -\bar{\epsilon}_{41}I + \check{D}_1^T \check{D}_1 \end{bmatrix},$$

$$\Theta_2 = \begin{bmatrix} \Theta_{11}^2 & P_{d2}(\check{E} - \check{\Gamma}_q \check{D}) + \check{G}^T \check{D}_2 + \check{C}^T \check{D}_2 \\ * & -I_\epsilon + \check{D}_2^T \check{D}_2 \end{bmatrix},$$

$$\Theta_{11}^1 = P_{d1}(A_q + BK_q) + (A_q + BK_q)^T P_{d1} + (\gamma + 1)C^T C,$$

$$\Theta_{11}^2 = P_{d2}(\check{A}_q - \check{\Gamma}_q \check{C}) + (\check{A}_q - \check{\Gamma}_q \check{C})^T P_{d2} + \gamma^{-1} \check{G}^T \check{G} + \check{P}_d,$$

$$\Theta_{14}^1 = P_{d1}[E \quad I] + C^T \check{D}_1, \quad \check{P}_d = \text{diag}\{\check{Y}_1, \check{Y}_2\} + \check{C}^T \check{C}. \quad (42)$$

To address condition (40), the matrix $U = \text{diag}\{\bar{P}_{d1}, \bar{P}_{d1}, I, I\}$ is assigned, where $\bar{P}_{d1} = P_{d1}^{-1}$. A congruent transformation is then applied to the matrix Θ_1 with U . By applying the Schur complement lemma, condition (31) ensures that (40) is satisfied. For condition (41), setting $\check{\Gamma}_q = P_{d2} \check{\Gamma}_q$ allows the remaining steps in the proof to be completed by following the approach outlined in Theorem 1. This completes the proof. ■

V. EXPERIMENTS

Experimental verifications are conducted to demonstrate the effectiveness of the proposed diagnostic and tracking framework. The hardware-in-the-loop (HIL) real-time experimental platform, shown in 3, integrates several key components. The

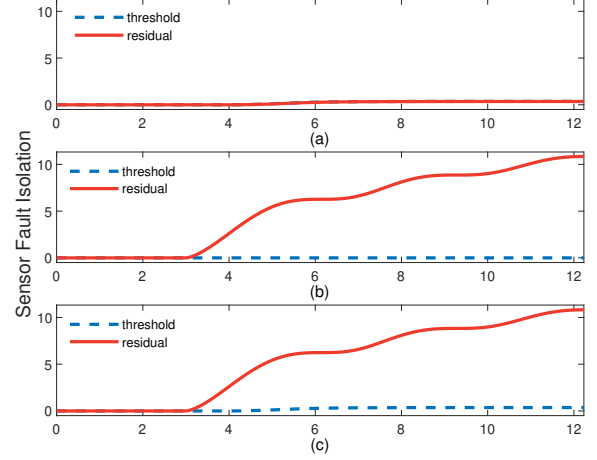


Fig. 5. Evaluation function of $\mathbb{J}_1(e_y)$ under different fault scenarios. (a) Only actuator fault; (b) Only sensor fault; (c) Both sensor and actuator faults.

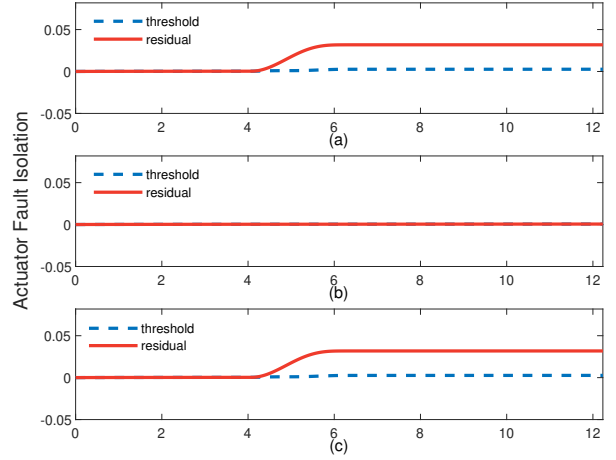


Fig. 6. Evaluation function of $\mathbb{J}_2(e_y)$ under different fault scenarios. (a) Only actuator fault; (b) Only sensor fault; (c) Both sensor and actuator faults.

control equipment consists of a wheel speed test bench, a real-time simulation computer, a host computer, and associated management software. Communication with the wheel speed test bench system is facilitated via the EtherCAN Bus. The simulation computer is dedicated to model computation, receiving control signals through the reflective memory network, and outputting model parameters for interaction with other subsystems. Data acquisition is handled by a device that collects electrical signals from the panel and fault injection unit, retrieves model data via the reflective memory network, and transmits it to the integrated control equipment by high-speed Ethernet. The host computer, which receives aircraft model state signals through high-speed Ethernet, is responsible for monitoring and managing the entire system.

The conformity parameters utilized in this experiment test are as follows: $M = 5000$ kg, $h = 1.878$ m, $a = 2.328$ m, $b = 4.68$ m, $T_i = 426$ N, $k_v = 1$ N·s/m, $\rho = 1.203$ kg/m³, $C_x = 0.1029$, $S_w = 31$ m², $g = 9.8$ N/kg, $C_z = 0.359$,

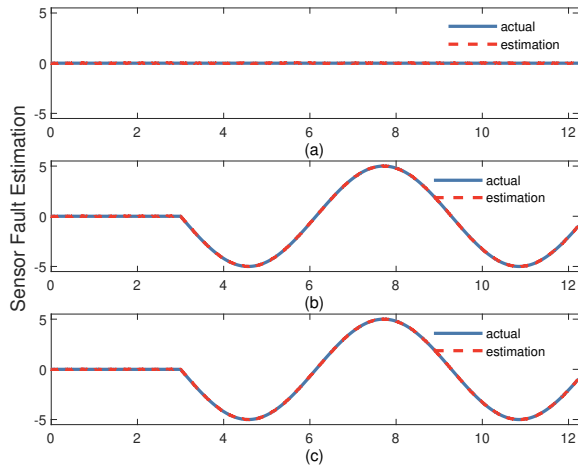


Fig. 7. Estimated and actual values of $f_s(t)$ under different fault scenarios. (a) Only actuator fault; (b) Only sensor fault; (c) Both sensor and actuator faults.

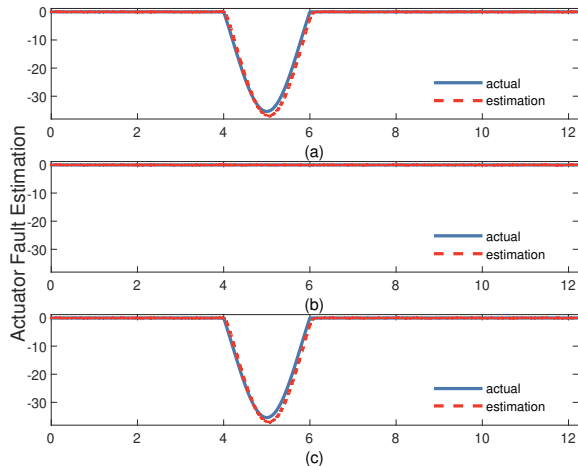


Fig. 8. Estimated and actual values of $f_a(t)$ under different fault scenarios. (a) Only actuator fault; (b) Only sensor fault; (c) Both sensor and actuator faults.

$h_t = 0.1$ m, $R = 0.3$ m. The aircraft initiates braking upon landing at a speed of $v_x(0) = 72$ m/s, with the main wheels initially rolling freely at $w_r(0) = 240$ rad/s. To validate the capability in handling simultaneous actuator and sensor faults of the proposed fault isolation and fault-tolerant control method, tests are conducted under three scenarios: (a) actuator fault only; (b) sensor fault only; and (c) simultaneous actuator and sensor faults. The fault conditions are set as follows: the actuator fault is injected as a transient fault, occurring between 4-6 seconds, while the sensor fault is an oscillatory fault, starting at 3 seconds and persisting until the end of the experiment.

Fig.4 illustrates the membership functions of the system, observer, and controller during operation. The shaded regions, depicted in different colors, represent the relative errors in membership degrees between the system and the observer or controller. The light blue region corresponds to relative

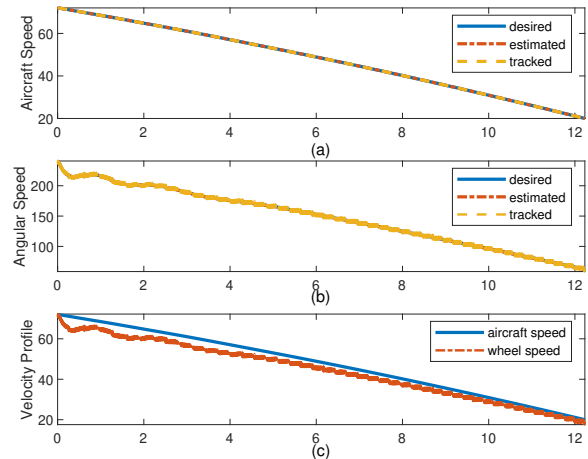


Fig. 9. Comparison of aircraft speed and wheel speed signals.

errors within the range of 0 to 0.005, the dark blue region captures relative errors between 0.005 and 0.0075, and the red region indicates relative errors exceeding 0.0075. The figure highlights two key observations. First, a persistent relative error exists between the membership functions of the observer and the system, primarily due to sensor faults and modeling uncertainties. Second, despite the presence of these errors, the observer maintains estimation accuracy by ensuring that the relative errors remain bounded within a reasonable range. This behavior is consistent with the bounded deviation assumption discussed in Section III and underscores the robustness of the proposed method. Figs. 6-8 display the isolation and estimation results for three different fault scenarios, with subfigures (a), (b), and (c) corresponding to actuator faults, sensor faults, and simultaneous actuator and sensor faults, respectively. The experimental results indicate that the proposed method effectively diagnoses and reconstructs specific faults while remaining insensitive to non-specific faults. Fig. 9 presents the fault-tolerant control results, showing that even under dual fault conditions, the controller can still ensure that the EABS accurately tracks the desired targets, achieving satisfactory braking performance. From the results above, it can be observed that the proposed method effectively reconstructs and compensates for the impact of faults, and stabilizes the closed-loop system performance.

VI. CONCLUSION

This paper presents a comprehensive framework for fault isolation, estimation, and fault-tolerant control of aircraft EABS under actuator and sensor fault conditions. To address the inherent nonlinearity of the EABS, a T-S fuzzy model is developed to achieve global approximation of time-varying dynamics. By utilizing mismatched premise variables and the output equivalence principle, an asynchronous T-S fuzzy observer is designed to estimate both actuator and sensor faults simultaneously. Based on the fault estimation, an integrated fault-tolerant control strategy is proposed. This control system uses the estimated fault information to ensure effective fault

compensation and maintain the desired performance of the EABS even in the presence of faults. Experimental results confirm the practical applicability of the proposed framework, demonstrating its effectiveness in real-time fault estimation and fault-tolerant control. One direction for future work is the development of knowledge-driven and data-derived intelligent fault diagnosis and modulation mechanism.

REFERENCES

- [1] X. Yao, B. Zhao and S. Li, "Disturbance observer-based tracking control of high-speed trains under adhesion dynamics," *IEEE Trans. Autom. Sci. Eng.*, vol. 21, no. 2, pp. 1727-1739, Apr. 2024.
- [2] L. Zhu, D. Huang, X. Li and Q. Wang, "Cooperative operation control of virtual coupling high-speed trains with input saturation and full-state constraints," *IEEE Trans. Autom. Sci. Eng.*, vol. 21, no. 3, pp. 3497-3510, Jul. 2024.
- [3] M. Forghani, J. M. McNew, D. Hoehener and D. D. Vecchio, "Design of driver-assist systems under probabilistic safety specifications near stop signs," *IEEE Trans. Autom. Sci. Eng.*, vol. 13, no. 1, pp. 43-53, Jan. 2016.
- [4] Z. Jiao, N. Bai, D. Sun, X. Liu, J. Li, Y. Shi, Y. Hou, and C. Chen, "Aircraft anti-skid braking control based on reinforcement learning," *IEEE Trans. Aerosp. Electron. Syst.*, vol. 59, no. 6, pp. 9219-9232, Dec. 2023.
- [5] R. Li, W. Qiao, X. Liu, H. Jin, X. Gao, D. Li, S. Wu, Y. Shang, and Z. Jiao, "A novel dual-redundancy more-electric braking system and regulation strategy based on on/off valves," *IEEE/ASME Trans. Mechatronics*, vol. 29, no. 6, pp. 4594-4605, Dec. 2024.
- [6] L. D'Avico, M. Tanelli, and S. M. Savaresi, "Tire-Wear Control in Aircraft via Active Braking," *IEEE Trans. Control Syst. Technol.*, vol. 29, no. 3, pp. 984-995, May 2021.
- [7] J. Deja, I. Dayyani, V. Nair, and M. Skote, "More electric aircraft conversion to all-electric during ground operations: battery-powered landing gear drive system," *IEEE Trans. Transp. Electr.*, vol. 10, no. 1, pp. 744-759, Mar. 2024.
- [8] H. Hussaini, T. Yang, G. Bai, M. Urrutia-Ortiz, and S. Bozhko, "Artificial intelligence-based hierarchical control design for current sharing and voltage restoration in dc microgrid of the more electric aircraft," *IEEE Trans. Transp. Electr.*, vol. 10, no. 1, pp. 566-582, Mar. 2024.
- [9] Z. Wang, X. Liu, D. Sun, N. Bai, P. Qi, and Z. Jiao, "A real-time maximum tire-road friction tracking control method for aircraft braking system with disturbance compensation," *IEEE/ASME Trans. Mechatronics*, vol. 29, no. 5, pp. 3649-3660, Oct. 2024.
- [10] A. d. O. Gomes and J. C. Basilio, "A fuzzy inference model to identify the current industry maturity stage in the transformation process to Industry 4.0," *IEEE Trans. Autom. Sci. Eng.*, vol. 21, no. 2, pp. 1607-1622, Apr. 2024.
- [11] T. A. Nguyen, "Development of a novel integrated control strategy for automotive electric power steering systems," *IEEE Trans. Autom. Sci. Eng.*, Early Access, doi: 10.1109/TASE.2024.3356509.
- [12] F. Santoso, M. A. Garratt and S. G. Anavatti, "State-of-the-Art intelligent flight control systems in unmanned aerial vehicles," *IEEE Trans. Autom. Sci. Eng.*, vol. 15, no. 2, pp. 613-627, Apr. 2018.
- [13] Z. Hou, Z. Li, C. Hsu, K. Zhang and J. Xu, "Fuzzy logic-driven variable time-scale prediction-based reinforcement learning for robotic multiple peg-in-hole assembly," *IEEE Trans. Autom. Sci. Eng.*, vol. 19, no. 1, pp. 218-229, Jan. 2022.
- [14] S. Yan, W. Sun and Y. Xia, "A joint fault-tolerant and fault diagnosis strategy for multiple actuator faults of full-vehicle active suspension systems," *IEEE Trans. Autom. Sci. Eng.*, Early Access, doi: 10.1109/TASE.2024.3372626.
- [15] S. Roshanravan and S. Shamaghdari, "Adaptive fault-tolerant tracking control for affine nonlinear systems with unknown dynamics via reinforcement learning," *IEEE Trans. Autom. Sci. Eng.*, vol. 21, no. 1, pp. 569-580, Jan. 2024.
- [16] X. Gong, J. Gui, Y. Chen, X. Yang, W. Yu and T. Huang, "Resilient human-in-the-loop formation-tracking of multi-UAV systems against byzantine attacks," *IEEE Trans. Autom. Sci. Eng.*, early access, doi: 10.1109/TASE.2024.3400155.
- [17] S. Langarica, C. Ruffelmacher and F. Núñez, "An industrial internet application for real-time fault diagnosis in industrial motors," *IEEE Trans. Autom. Sci. Eng.*, vol. 17, no. 1, pp. 284-295, Jan. 2020.
- [18] K. Zhang, B. Jiang, X. Yan, Z. Mao, and M. M. Polycarpou, "Fault-tolerant control for systems with unmatched actuator faults and disturbances," *IEEE Trans. Autom. Control*, vol. 66, no. 4, pp. 1725-1732, Apr. 2021.
- [19] X. Zhang, "Sensor bias fault detection and isolation in a class of nonlinear uncertain systems using adaptive estimation," *IEEE Trans. Autom. Control*, vol. 56, no. 5, pp. 1220-1226, May 2011.
- [20] F. Jia, J. Huang and X. He, "Predefined-time fault-tolerant control for a class of nonlinear systems with actuator faults and unknown mismatched disturbances," *IEEE Trans. Autom. Sci. Eng.*, vol. 21, no. 3, pp. 3801-3815, Jul. 2024.
- [21] A. A. Ladel, A. Benzaouia, R. Outbib and M. Ouladsine, "Integrated state/fault estimation and fault-tolerant control design for switched T-S fuzzy systems with sensor and actuator faults," *IEEE Trans. Fuzzy Syst.*, vol. 30, no. 8, pp. 3211-3223, Aug. 2022.
- [22] J. Qiu, Y. Wei, and L. Wu, "A novel approach to reliable control of piecewise affine systems with actuator faults," *IEEE Trans. Circuits Syst. II, Exp. Briefs*, vol. 64, no. 8, pp. 957-961, Aug. 2017.
- [23] K. Sun, L. Liu, J. Qiu, and G. Feng, "Fuzzy adaptive finite-time fault-tolerant control for strict-feedback nonlinear systems," *IEEE Trans. Fuzzy Syst.*, vol. 29, no. 4, pp. 786-796, Apr. 2021.
- [24] X. Yao, L. Wu, and L. Guo, "Disturbance-observer-based fault tolerant control of high-speed trains: A markovian jump system model approach," *IEEE Trans. Syst., Man, Cybern.: Syst.*, vol. 50, no. 4, pp. 1476-1485, Apr. 2020.
- [25] R. Ma, H. Zhang, M. Yuan, B. Liang, Y. Li, and Y. Huangfu, "Chattering suppression fast terminal sliding mode control for aircraft EMA braking system," *IEEE Trans. Transp. Electr.*, vol. 7, no. 3, pp. 1901-1914, Sep. 2021.
- [26] N. Bai, X. Liu, J. Li, Z. Wang, P. Qi, Y. Shang, and Z. Jiao, "An aircraft brake control algorithm with torque compensation based on RBF neural network," *Chin. J. Aeronaut.*, vol. 7, no. 1, pp. 438-450, Jan. 2024.
- [27] J. J. M. Lopetegui, G. Papa, M. Morandini, and M. Tanelli, "Data-driven modeling and regulation of aircraft brakes degradation via antiskid controllers," *IEEE Trans. Rel.*, vol. 72, no. 3, pp. 889-899, Sep. 2023.
- [28] M. Gerard, W. Pasillas-Lépine, E. de Vries, and M. Verhaegen, "Improvements to a five-phase ABS algorithm for experimental validation," *Veh. Syst. Dyn.*, vol. 50, no. 10, pp. 1585-1611, Oct. 2012.
- [29] W. Pasillas-Lépine and M. Gerard, "Design and experimental validation of a nonlinear wheel slip control algorithm," *Automatica*, vol. 48, no. 8, pp. 1852-1859, Aug. 2012.
- [30] Z. Jiao, D. Sun, Y. Shang, X. Liu, and S. Wu, "A high efficiency aircraft anti-skid brake control with runway identification," *Aerosp. Sci. Technol.*, vol. 91, pp. 82-95, Aug. 2019.
- [31] M. Chadli, A. Abdo, and S. X. Ding, " $\mathcal{H}_2/\mathcal{H}_\infty$ fault detection filter design for discrete-time Takagi-Sugeno fuzzy system," *Automatica*, vol. 49, no. 7, pp. 1996-2005, Jul. 2013.



Yiyun Zhao received the B.E. and Ph.D. degrees in electrical engineering from North.western Polytechnical University, Xi'an, China, in 2017 and 2024, respectively. In 2024, he joined the Central South University, as a Lecturer. His research interests include more electric aircraft, nonlinear control, and mechatronic servo control.



Zheng Wu received the B.S. degree in automation from Hebei University of Technology, Tianjin, China, in 2018, and the M.S. degree in control science and engineering from Central South University, Changsha, China, in 2021. He is now working for a Ph.D. degree in Control Science and Engineering in Central South University, Changsha, China. Since September 2024, he has been a Visiting Scholar with the Power Electronics, Machines, and Control Group at the University of Nottingham, U.K.

His research interests include aircraft braking system, sliding mode control, and fuzzy logic systems.



Weihua Gui (Member, IEEE) received the B.Eng. degree in electrical engineering and the M.Eng. degree in automatic control engineering from Central South University in 1976 and 1981, respectively. From 1986 to 1988 he was a Visiting Scholar at Universität-GH-Duisburg, Germany. Since 1991, he has been a Full Professor at Central South University. Since 2013, he has been an Academician with the Chinese Academy of Engineering. His main research interests include modeling and optimal control of complex industrial process, distributed robust control, and fault diagnoses.

control, and fault diagnoses.



Fanbiao Li (Senior Member, IEEE) received the B.S. degree in applied mathematics from Mudanjiang Normal University, Mudanjiang, China, in 2008, the M.S. degree in operational research and cybernetics from Heilongjiang University, Harbin, China, in 2012, and the Ph.D. degree in control theory and control engineering from the Harbin Institute of Technology, Harbin, in 2015.

From April 2015 to February 2016, he was a Research Associate with the School of Electrical and Electronic Engineering, The University of Adelaide. From July 2016 to June 2020, he was an Associate Professor with Central South University, Changsha, China. From April 2017 to March 2018, he was an Alexander von Humboldt Research Fellow with the University of Duisburg–Essen, Duisburg, Germany. He is currently a Full Professor with Central South University. His research interests include control and design of aircraft brake system, sliding-mode control, and fault diagnosis and identification. Prof. Li currently serves as an Associate Editor for a number of journals, including IEEE Transactions on System, Man, and Cybernetics: Systems, IEEE Transactions on Fuzzy Systems, etc.



Tao Yang (Senior Member, IEEE) received the M.Eng. degree from Shanghai Jiao Tong University, Shanghai, China, in 2008, and the Ph.D. degree in electrical engineering from the University of Nottingham, Nottingham, U.K., in 2013. Since 2013, he has been a Researcher with the Power Electronics, Machines and Control Group, University of Nottingham, where he became an Assistant Professor in 2016, and an Associate Professor in 2019. His research interests include high-speed electric motor drive control, power electronic conversion, electrical

system design, and optimization for more electric/hybrid/all-electric aircraft applications. His Ph.D. research within EU Clean Sky on Modeling electrical power system for more-electric aircraft applications has resulted in him winning the inaugural Clean Sky Best Ph.D. Award in 2016. He is an Associate Editor for the IEEE Transactions on Transportation Electrification and Chinese Journal of Aeronautics.



Chunhua Yang (Fellow, IEEE) received the M.Eng. degree in automatic control engineering and the Ph.D. degree in control science and engineering from Central South University, Changsha, China, in 1988 and 2002, respectively. She was with the Department of Electrical Engineering, Katholieke Universiteit Leuven, Leuven, Belgium, from 1999 to 2001. She is currently a Full Professor with Central South University. Her current research interests include modeling and optimal control of complex industrial processes, intelligent control systems, and

fault-tolerant computing of real-time systems. She serves as an Associate Editor for a number of journals, including IEEE Transactions on Industrial Electronics, IEEE/ASME Transactions on Mechatronics. She is a fellow of IEEE.